

## 2 METHODOLOGICAL AND INSTRUMENTAL RESEARCH



## 2.1 SEISMIC METHODOLOGICAL AND INSTRUMENTAL RESEARCH

### 2.1.1 VIBROSEIS® methodological experiments\*

In the 1984 Annual Report of ELGI we have already presented the first results of the high frequency VIBROSEIS® measurements which have demonstrated that the application of combined sweeps improves the quality. In 1985, combined sweeps were used in the detailing phase of the geophysical exploration of the brown coal field of Mány-K-Zsámbék. As a result of the experimental measurements effected in the area, a high-frequency, combined sweep was used, consisting of 3 linear components, with frequency ranges of 40–200 Hz, 60–200 Hz and 80–200 Hz, respectively. The sections were of good quality, and by accurately reflecting the geological structure of the area, have facilitated to a considerable extent the planning of subsequent research objectives.

As an example, we present the migrated time section GV-10, coloured according to amplitude strength (*Fig. 48*). From the section, the dip conditions of the various formations and the positions of the structural elements are clearly definable. A good example is the changing dip conditions of the Miocene formations. The undisturbed horizontal strata assume an approximately 20° dip to the west from point 5°. Between boreholes Ma-211 and Ma-262 a tectonic zone may be observed, resulting in a displacement of several hundred metres amplitude. The eastern edge of this zone is the main fault whereas to the west a multi-staged system of faults had developed. The quality of the section is superior to any sections recorded previously in this area either by VIBROSEIS®, or by explosion seismics. For comparison, see the segment between 2.5–3.5 kilometres of the time section of *Fig. 6* of Annual Report for 1982. The two sections run almost parallel to each other, at a distance of 100–200 metres. Comparing the information contents of the two sections it may be stated that—with identical processing—both the horizontal and vertical resolutions, and the signal/noise ration of section GV-10 are superior.

The favourable experiences with the combined sweeps led us to further experiments. We wanted to compare the effects of the combined sweeps with that of the programmed non-linear sweeps. With non-linear sweeps, the spectrum of input signals can be tuned in a very precise manner, the actual

---

\* György L.

frequency and amplitude of the signal may be determined at 8 ms intervals. It is a further advantage of the non-linear sweeps that the amplitude attenuation of high frequencies of the linear components of the combined sweeps can also be eliminated. A definite disadvantage is that sweeps cannot be tuned in the field, they have to be set in laboratory conditions.

Our experimental measurements have been carried out in the brown coal field of Mány-K-Zsámbék. Reflection profile K-7/85 was recorded with two different sweep types: K-7A/85 (Fig. 49/a) with the application of a combined sweep consisting of 4 linear sweeps having the frequency ranges of 30-130 Hz, 40-140 Hz, 50-150 Hz and 60-160 Hz, respectively, while K-7C/85 (Fig. 49/b) with a non-linear sweep, following the function  $f_t = 30 + 9t + 5 \sin\left(2\pi \frac{t}{14}\right)$ . The *theoretical* amplitude spectra of the sweeps are shown in Figs. 50 and 51, while the amplitude spectra of the actual seismic traces belonging to points 500 and 1000 m in Figs. 52 and 53, respectively. They are normalized mean average spectra of ten seismic traces. From the last two figures it can be seen, that spectra depend both on the type of the sweep and on the low-velocity layer. At point 1000 the spectrum of the seismic trace has a lower frequency content, which is the result of the high-frequency filtering effect of the thick low-velocity layer. Another readily apparent fact is that the non-linear sweep has a broader spectrum, the high frequencies are stronger, than in the case of the combined sweep. This is the result of the amplitude attenuation of the linear components of the combined sweep at high frequencies, which does not occur in the case of the non-linear sweep.

Comparing the two time sections it is found that the thinning of the Eocene, containing the coal-bearing layers, towards the main fault can be seen in that version only, which was recorded by the non-linear sweep. The inner structure of the Oligocene is somewhat reflecting in that same version.

The reasons for this can be found in the differences of the spectra. As a result of the first experiments it may be stated, that the introduction of non-linear sweeps to targets needing high resolution could probably result in further progress.

In the course of our previous surveys we have frequently found ourselves in the situation, where the correctly regulated vibrators—moving into differing surface conditions—produced distorted sweeps. These distorted sweeps may lead to the extensive distortion of the Klauder wavelet, considerably deteriorating the signal-to-noise ratio of time sections. To eliminate this effect the American Pelton Company has developed the so-called Force Control unit which, in the case of inadequate soil-vibrator contact, automatically regulates vibrator force. This system ensures distortion-free sweeps, regardless of surface conditions.

In 1985 we have carried out some experimental measurements with a Force

Control unit, by attaching an accelerometer to the baseplate of the vibrator. In *Fig. 54* amplitudes and phase distortions of sweeps are demonstrated after arriving at an asphalt road from the field, for which the vibrators were properly set. It can be seen that in normal mode both amplitude and phase show considerable distortion, especially in the frequency range of 65–100 Hz. These distortions are eliminated with the use of the Force Control. As a result of these tests, we have purchased, together with the high frequency vibrators, the Force Control unit, as well. Regular use of this equipment will commence in 1986.

### **2.1:2 Computer processing of in-mine seismic transmission\***

In Annual Report for 1981 it has already been indicated that the level of accumulated theoretical and practical knowledge allowed the actual commencement of in-mine seismic measurements. During the last four years the in-mine geophysical survey has become a regular activity, an integral part of the geological–geophysical exploration.

One of the most important and most widely used method of in-mine seismics is the seam wave transmission which is used for checking the seams prepared for mining for tectonic disturbances. After the introduction of that technique, interpretation of seismograms has been carried out manually for years but the increasing quality requirements necessitated the development of computer processing.

The processing is based on the analysis of the SH component of the channel waves in the coal deposit—the so-called Evison waves. It is known that a significant part of the energy of low frequency components of Evison waves propagates outside of the seam in the form of inhomogeneous plane waves, while the energy of high frequency components is mainly concentrated within the seam. Thus if the wave guiding channel, i.e. the seam is interrupted by a disturbance of small amplitude, the energy loss of high frequency components propagating within the seam will be significantly larger than that of the low frequency components propagating mainly outside the seam. Thus from the point of view of Evison waves, faults can be regarded as high-cut filters, where the slope of the filter depends on the size of the fault. The slope of the filter of a fault e.g. of half seam throw is 4–8 dB/octave only, while that of a fault of throw larger than the thickness of the seam, can be as high as 20–40 dB/octave.

Analysing the spectra of the Evison waves, the presence of a filtering effect and its degree can be determined. From the first condition the existence of a fault, from the second its dimensions can be estimated. For the measure-

---

\* *Bodoky T.*, Hermann L.

ment of the filtering effect the so-called transmission coefficient has been introduced, which is the ratio of the energy of a high- and a low frequency band of the Evison wave. The transmission values along the boundary of the investigated area can be regarded as projections of transmission coefficients characteristic for the internal part of the area. Thus from the transmission values determined along the boundary of the area, the transmission map of the whole area can be calculated with a backprojection process.

The result of the computer processing of seam wave transmission is the transmission map, where faults are indicated by so-called "shadow zones". Dimensions of faults can be estimated more safely, if not only one transmission map is calculated, but a transmission map set for various upper frequency bands. On the transmission map belonging to the highest frequencies all the small disturbances are shown, while on those for the lower frequencies only faults of bigger size will be observed.

As an example of the computer processing of seam wave transmission one of our surveys in the Ménkes Colliery of the Nógrád Coal Mines are shown. *Figures 55 and 56* show two maps from the set, the first belonging to the so-called Airy frequency (320–380 Hz), the second to a lower band (260–320 Hz). *Figure 55* shows two parallel faults along the deposit. One of these, of 6.3 m throw was already known from roadway *C*. The transmission map shows the continuous reduction of its throw in the direction of roadway *A*, after which it is not detectable. The second fault was not known from the roadway, its strong shadow zone can be observed along roadways *B*.

On the map belonging to the lower frequencies (*Fig. 56*) the shadow of the first fault is obscure except in the vicinity of roadway *C*. This indicates that departing from roadway *C* its throw decreases fast. The shadow zone of the second fault is very clear on this map too, indicating a significant throw. Determination of the second fault led to stopping the mining activity, because winning of the tectonized deposit would not have been economical.

### **2.1.3 The geological section estimation (PGR) program package in seismic processing\***

A new version of the PGR (Prognozirovanie Geologicheskogo Razreza) elaborated by the Central Geological Expedition of the Ministry of Petroleum Industry of the Soviet Union (*Fig. 57*) has been adapted in 1985, which is integrated into the seismic digital processing system SDS-3 (see Ann. Report 1983). The PGR program package provides the following new possibilities for the user:

---

\* *Petrovics I., Majkuth T.*

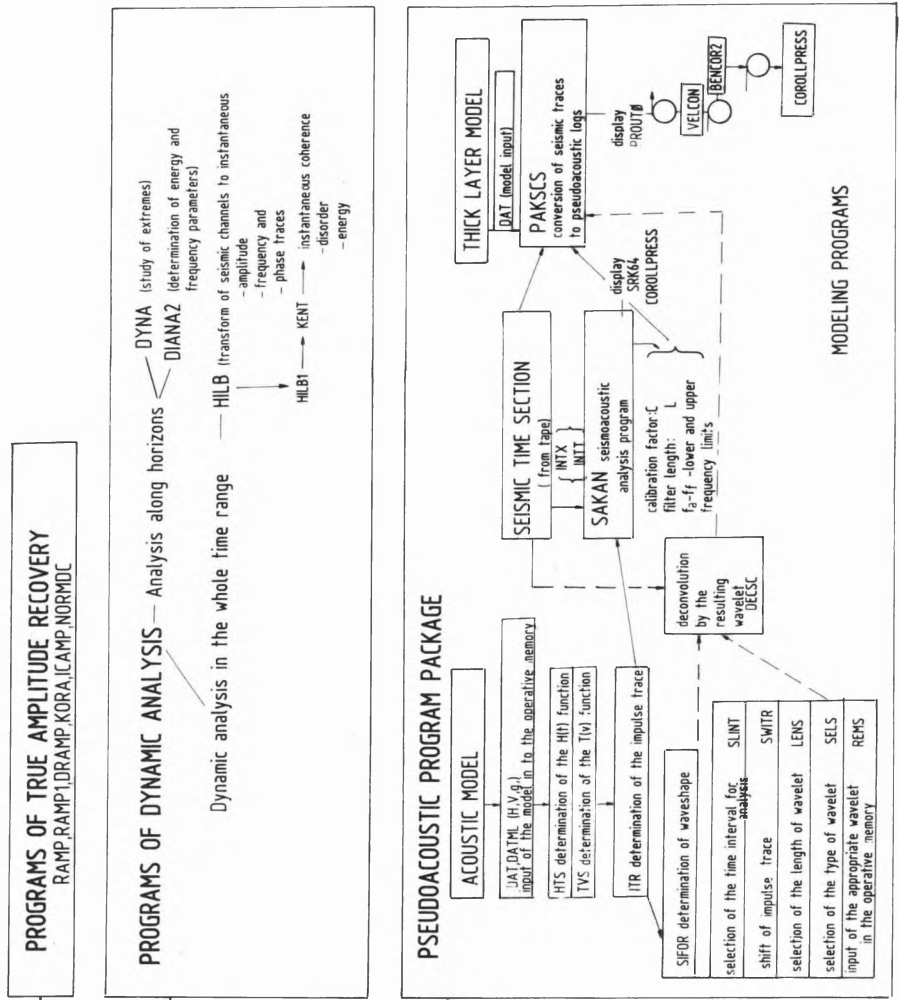


Fig. 57. Block scheme of PGR program package

- a) New programs for true amplitude recovery:
- amplitude correction according to surface effects
  - true amplitude recovery by compensating the spherical and absorption losses
  - gain control by a given function.

Among the true amplitude recovery programs the most suitable one is selected depending on the processing procedure and the seismogeological conditions of the area.

- b) Dynamic analysis of seismic records:
- dynamic analysis of seismic records in required intervals: energy and frequency spectra
  - dynamic analysis of seismic records in the complete time range; using the Hilbert transform in the time domain the seismic channels can be transformed to instantaneous amplitude-, frequency-, phase-, coherence-, disorder- and entropy traces.

The KENT program was fitted into the processing system operating by ELGI's array processor by our programmers.

- c) Possibilities of the PAK (pseudoacoustic log) program package:

- editing of acoustic logging data
- determination of the waveshape
- deconvolution
- seismoacoustic analysis
- pseudoacoustic transform

Results of the SAKAN (seismic analysis) are displayed by the colour plotter programs developed at ELGI. (For an example for the use of PAK, see: *Geophysical Transactions* **32**, 1, pp. 3–29.)

As an example, the dynamic analysis for the whole time range of the reflection profile Nsz-1/80 is presented. The profile was shot in the Nagygyháza brown coal basin in 1980 with the main purpose of determining the positions and dimensions of the structural elements. *Figure 58* shows the result of the routine processing: the migrated time section coloured according to amplitude strength. Further examples show the processing possibilities of PGR, i.e. the instantaneous amplitude (*Fig. 59*), the instantaneous frequency (*Fig. 60*) and the instantaneous entropy (*Fig. 61*). The structural features determined by integrating the results of the various processing procedures, checked by new boreholes and advancing galleries is shown on *Fig. 58*; further figures show those faults which appear best on that special section. It can be established that faults with throw higher than 5 m can be determined reliably (thick line). Faults of about 5 m amplitude (thin line) can be determined unambiguously, if the fault is young and affects the Eocene–Oligocene contact. Displacements between 1 and 5 m can be determined in exceptional cases only (indicated by dashed thin line).



#### 2.1.4 Seismic digital field system, model SD 16\*

The development of the latest member of the SD family of seismic field systems was completed in 1985. The result is an up-to-date high resolution computer controlled, 96 channel field instrument, developed—as well as the earlier SD 10, SD 12 and SD 20 models—in cooperation between ELGI and VEB Geophysik Leipzig, and its successor VEB Geophysikalische Gerätebau.

The block-scheme of *Fig. 62* represents the structure and operation of the instrument. Signals from geophones of a 144-channel spread are fed directly to the input. The function of the traditional “stacking” switch is provided by an electronic channel selector built into the input module. Signals of the selected 96 channels reach the amplifiers with non-transformer input. The formatting of analog signals is carried out by low-pass and high-pass filters and a notch filter rejecting the 50 Hz ac, which can be switched on or off. The seismic signals from the multiplexer get to the  $2 \times 48$  channel digital amplifier, and from here, they reach the A/D converter. The sorting of digital signals—after conversion—is ensured by a coupling circuit and a formatter in accordance with the recording requirements of the SEG B tape format. Digital signals can be sent to a correlator (VIBROSEIS<sup>®</sup> application) before the formatter and from the same point the reconverted analog signals can be recorded. After generating the suitable tape format, recording of digital signals is carried out by magnetic tape unit model MBS 161. Seismograms, written onto magnetic tape—after proper conversion—are displayed by an electrostatic matrix printer model ERG 21. The shooting encoder includes the generation of the start command and the circuits for receiving the time break and uphole signals.

The control system—based on a microcomputer model Robotron K 1520—consists of the CPU, the semiconductor memories required for the operation and the program storage, the operator pult, the CRT display indicating the information needed for operating and checking the instrument, the circuits generating the time-base for clock signals, the BUS system and—as auxilliary units—a cassette recorder and EPROM programmer.

The whole equipment occupies two cabinets, the first housing the tape unit model MBS 161, the electronic circuitry of the microcomputer model K 1520, the circuits of digital playback and their power supply. The second cabinet holds data acquisition system SDA III, containing the 96-channel analog amplifier and filter units, the time-variant stacking switch, the multiplexer, the digital amplifiers and A/D converters with their control, the optional analog playback circuits and the power supply.

The CRT display and the operator pult fixed on a separate desk are used for selecting programs and parameters from the menue and to start/stop

---

\* Nagy M.

programs. The computer keyboard, placed in the drawer of the desk, is used for programming or program modification only, therefore it is locked up during normal operation.

An electrostatic camera model ERG 21 belongs to the equipment. It is possible to connect a shot-generating code system (shot by radio) and an analog recorder. Interfacing of these optional units are in progress.

Apart from operating functions the equipment has numerous built-in checking facilities, including working conditions, peripherals, power supply unit, etc. Some of the most important test programs are as follows:

- recording and playback of the magnetic tape unit;
- for testing of parameters of the data acquisition system recording signals of a built-in test generator, testing of cables;
- checking of digital data with bit lamps;
- evaluation of test records by the built-in oscilloscope, or by entering the data to a computer.

Power ( $3 \times 220$  V) is supplied by a petrol-engine generator.

#### Basic technical characteristics

No. of seismic channels	24 or 48 or 96
Input of seismic channels	non-transformer, $R_{in} = 2 \times 5 \text{ k}\Omega$
Max. input voltage	$600 \text{ mV}_{eff}$ , at 18 dB gain
Equivalent input noise	$\cong 0.3 \mu\text{V}_{eff}$ , 36 dB gain
No. of auxiliary channels	5
Gain of seismic channels	
constant gain	18, 24, 30 or 36 dB
Automatic gain control	0 to 84 dB in 12 dB steps accuracy of steps is 0.1%
Harmonic distortion	$< 0.1\%$
Cross-talk isolation	$> 80 \text{ dB}$
Identity of seismic channels	less than 1%
Frequency range without filters	from 5 to 250 Hz
Filters	
low-cut filters	“OFF” -3 dB at 5 Hz 12, 17, 24 or 12, 24, 42 Hz (selectable by computer, however selection of other frequencies is available)
slope	12 dB/octave or 24 dB/octave
50 Hz notch filter	-3 dB at 45 and 55 Hz -40 dB at 49.4 and at 50.5 Hz (it can be switched on by computer)

A/D converter	13 bits+ sign
linearity	0.1%
Recording	
tape format	PE, 1600 bit/inch
tape reel diam.	∅216 mm
Operating temperature range	+ 10... + 50 °C
Relative air humidity	10...95%

### 2.1.5 Engineering seismic processor model ESP\*

Instruments developed by ELGI for engineering-seismic (ESS-01-24) and in-mine seismic (SSS-1) measurements record data on standard (Philips type) magnetic cassettes in digital format. Data for processing can be entered into computers having cassette input facility. To meet the following requirements, set by users of our instruments, the pre-processing unit model ESP-1 has been developed. Requirements:

- to ensure the quality control of field materials at the field base, after finishing daily measurements. Thus repetitions and modifications of field parameters can be carried out economically;
- to create the possibility of transforming data recorded on cassette to 9 track magnetic tape format, which is widely used for input in processing centres.

Our goal was to satisfy the requirements by a programmable unit, bearing in mind its further development by means of programming without significant modification of the hardware configuration. Structure of the pre-processing unit and its modules are presented in *Fig. 63*.

Basic units of the hardware configuration:

- CPU, consisting of an 8-bit microprocessor, a 64 kbyte data storage, a 44 kbyte operative memory, peripheral interfaces for a magnetic cassette drive, a 9 track tape drive, a thermorecorder and a CRT display. By means of thumb-wheel switches on the CPU's operator pult modes of operation and parameters can be set. The CPU includes the magnetic cassette transport as well as the CRT displaying seismograms;
- standardised 9-track, 800 bpi NRZI-write magnetic tape drive;
- thermorecorder for drawing of seismograms on thermo-sensitive paper.

---

\* Czifra F.

## Main modes of operation:

- calling of menus onto the graphic display;
- reading seismograms from magnetic cassette into the operative memory (in its present configuration handling of formats ESS-01-24 and SSS-1 is possible);
- display of seismograms on the graphic screen;
- function modifying operations, like amplitude increasing/decreasing, application of program gain control by an exponential function;
- recording and automatic transfer from magnetic cassette to magnetic tape;
- registration of seismogram on thermorecorder.

## 2.2 GEOELECTRIC METHODOLOGICAL AND INSTRUMENTAL RESEARCH

### 2.2.1 Introduction, development and application of the transient method in Hungary\*

#### *Necessity of the introduction of the method in Hungary*

In Hungary the bauxite and coal exploration frequently requires the detection of small-size structures under inhomogeneous overburden. This determines the task of the methodological development in geophysics: geophysical methods of high vertical and horizontal resolution should be developed which are economic as well, i.e. large areas can be explored at relatively low costs.

The above requirements could be presumably met by the transient, i.e. time-domain electromagnetic method and its various measuring techniques. To test the possibilities, experimental measurements were carried out over domestic bauxite deposits with the help of foreign measuring parties (instruments used: Geonics EM-37, Sirotem-II, Impulse-C, Crone PEM). The EM-37/3 type instrument of Geonics Ltd. (Toronto, Canada) was found to be the most suitable for our purposes. The equipment was put into operation in February, 1985, and is used ever since. A data processing program package was written for the microcomputer supplied with the instrument (HP 85B) which is suitable for field use too. This program ensures fast processing of data. A new interpretation method, unknown in the literature, was elaborated. Finally, experimental measurements proved the suitability of the transient method for solving the exploration tasks.

#### *Theoretical basis of the transient method*

When using the transient method, direct current is fed into an insulated loop laid on the surface or to a pair of electrodes (transmitter) (*Fig. 64/a*) which induces a magnetic field (primary field). After turning off the current, the collapsing magnetic field induces eddy currents in the layers of the half-space, and these currents induce a rapidly decaying secondary magnetic field on the surface that is characteristic to the resistivity distribution (*Fig. 64/b*). By measuring

---

\* Balog Gy., Kakas K., Prácsér E., Sörös L., Újszászi J.

the components of the secondary magnetic (transient) field using a small induction loop, the geoelectric model of the half-space can be derived from the decay curve.

In practice, instead of the direct current, a train of bipolar pulses is used and several thousands of transient signals are stacked to improve the signal-to-noise ratio. The transient signal (decay curve) is sampled at logarithmically equal time intervals (*Fig. 64/c*). The Geonics EM-37/3 instrument has 30 sampling times (channels) between 80  $\mu$ s and 80 ms.

The computer programs developed in ELGI can be used for the calculation of the transient field above a layered half-space for the transmitter-receiver configurations of *Fig. 65*:

- a) Coaxial or CIL (central induction loop) configuration (strict transient sounding); the field is measured at the midpoint of the induction coil or loop, lying on the surface of the half-space;
- b) Turam configuration (or roving receiver transient mapping); the field of a rectangular loop lying on the surface is measured at an arbitrary surface point;
- c) Dipole-dipole (or Slingram) configuration, the field of a horizontal loop, equivalent with a magnetic dipole with vertical axis, is measured in the plane of the loop.

Instead of the measured decay curves, or the calculated field components, generally it is more expedient to analyse the apparent resistivity values derived from them. During the calculation of the resistivity, parameters of the measurement (the magnetic moments of the transmitter and receiver, and their mutual position) are taken into account and their effects are removed from the decay curves.

For a better understanding and development of the theoretical basis of the transient method and its interpretation the following works have been carried out in recent years:

- programs were written for the calculation of the transient field over horizontally layered half-space by using the inverse Fourier transform to the results of calculations in the frequency domain [PRÁCSER et al. 1983];
- programs for field calculations obtained from the USGS in the framework of the American-Hungarian technical-scientific cooperation (ANDERSON 1982) were further developed, the asymptotic calculation of values belonging to late times was made more simple and accurate;
- a fast resistivity calculating algorithm, using the inversion of field values, was elaborated. It is valid for all three configurations.

The theoretical field calculations and the resistivity calculating algorithm is discussed in another paper (PRÁCSER 1987).

Interpretation methods provide geoelectric parameters of horizontally layered media. Generally two procedures are widely used. The interpretation with theoretical curves determines the thicknesses and resistivities of the layers by comparison with two- and three-layer master curves. Similarly to the interpretation of vertical electric soundings the method is tedious even for three layers. The automatic inversion is basically a computer program which—starting from an initial guess—determines the theoretical curve approximating the measured one within given accuracy by iterations. These programs, e.g. those based on the Marquardt algorithm, however, run very slowly even on a main-frame computer. The disadvantage of both procedures is that the interpretation does not provide any information on the deviations from the horizontally layered model (horizontal inhomogeneities) and thin layers are difficult to follow. To improve and speed up interpretation a new procedure was elaborated by a transformation, which can be used for the determination of the apparent resistivity–apparent depth curve from the apparent resistivity–time curve (transient sounding curve). It can be proved, that for simple models, the intersections of the tangents of the resistivity–depth functions give the layer boundaries with good approximation. This depth calculation is called TRH inversion, because the conversion between time (T) and depth (H) is made through the resistivity (R).

The TRH inversion utilizes that property of the transient field that the most characteristic parameter of the current distribution is

$$\alpha = \frac{t\rho}{H^2}$$

This property has already been recognized by several authors [NABIGHIAN 1979, RAICHE and GALLAGHER 1985]. Based on this, penetration depth  $H_{eff}$  can be defined for transient fields, which can be visualized as the instantaneous depth of a “radiating smoke ring” below the transmitter:

$$H_{eff} \sim \sqrt{t\rho}$$

In inhomogeneous half-space it is useful to define the apparent depth  $H_A$  as the instantaneous depth of the “smoke ring” in a homogeneous half space; thus:

$$H_A = C_r \sqrt{t\rho_A}$$

where  $\rho_A$  is the apparent resistivity at moment  $t$  and  $C_r$  can be regarded constant for a given transmitter–receiver configuration.

The TRH procedure, even together with the resistivity calculation, can be carried out rather simply, thus providing a possibility for fast and automatic interpretation. If it is used in combination with graphic or Marquardt inversion methods, resistivities of the layers can also be determined.

The data acquisition, correction and processing program package (Fig. 66) was developed by adapting the programs of Geonics—applied in ore exploration—to our exploration tasks. It comprises exact and fast resistivity calculation, plotting of the sounding curves necessary for the graphic interpretation and, of course, the TRH inversion.

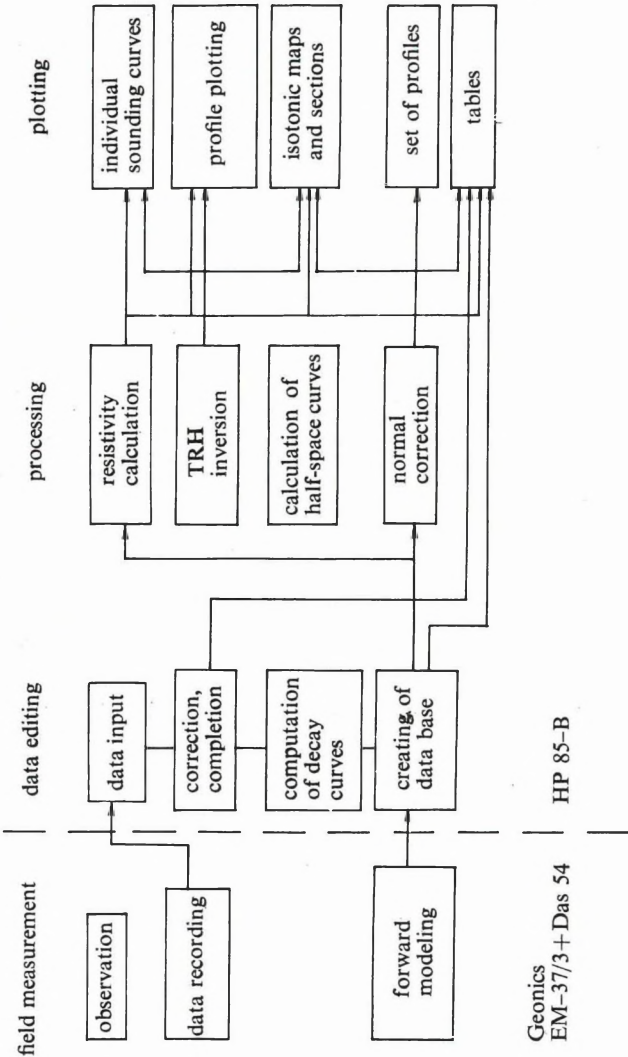


Fig. 66. Flow chart of transient data processing



The first step in the data processing is the recording of measured data. In practice 200–20,000 decay curves are stacked to reduce the measuring errors and to improve the signal-to-noise ratio. Still, the measurement of a transient curve is much faster than any other sounding procedure — if the time required for laying out the transmitter loop is not considered. In order to keep this advantage, the Geonics EM–37/3 instrument stores the data in a 32 kbyte solid state memory data logger, from where data are transferred to a HP 85B micro-computer operated in the field office.

After the required corrections (e.g. errors in the headers) and additions (transmitter current, loop size), raw field data are transferred to the data tape. After that, the so-called combined curves are calculated from the information of recordings made at the same station but using different polarities and transmitter frequencies. Further processing comprises apparent resistivity calculations for all three configurations, displaying of the processed data in various forms (the  $B_z$  values, the  $\rho_A(t)$  and  $H_A(\rho_A)$  curves of each combined curve are plotted together with their scales) plotting of profiles ( $H_A(\rho_A)$ ) and isotonic maps.

#### *Examples for the application of transient measurements*

To demonstrate the results obtainable by the transient method, two examples are shown from our experimental measurements. The throw of the southwestern fault zone of the Iharkút–Németbánya bauxite deposits exceeds 500 m. Its exact detection is, however, made difficult by the increased resistivity of the Oligocene–Lower Miocene overburden above the fault zone (thus the fault cannot be detected by dc measurements). Further, the effect of the structural line is masked by rugged topography. From the TRH section, constructed from CIL soundings (*Fig. 67/a*), the fault can be determined. *Fig. 67/b* shows the resistivity–depth section calculated by the TRH procedure, that allows a fast qualitative interpretation. According to the interpretation of the two profiles, the depth to the downthrown Triassic basement can be determined as near as 100 m from the fault plane. This demonstrates the high lateral resolution of transient soundings. The reason for this is that as the decay curve is measured in the lack of primary field the receiver can be placed in the midpoint of the transmitter loop. By this “zero offset” configuration, the reference point problems of the electromagnetic measurements is avoided, the “investigated region” is definitely below the common axis of the transmitter and the receiver. *Fig. 67/c* shows the comparison of the CIL sounding curves measured on the two sides of the fault.

The Bakonyoszlop–X bauxite deposit was explored by drillings in a  $50 \times 50$  m grid. The bauxite, deposited at about 150 m depth, and the underlying terrestrial sequence fill a graben of the Triassic dolomite basement. The detec-

tion of the bauxite deposit was difficult using the traditional methods, because the effect of the medium-resistivity bauxite was screened by the inhomogeneous Oligocene–Lower Miocene overburden containing high-resistivity layers as well.

Above the bauxite deposit CIL soundings were carried out in a  $25 \times 25$  m grid and resistivity maps were constructed for different sampling times. Increasing the sampling time the penetration depth increases too, and an elongated low-resistivity zone appears, that could be identified as the effect of the bauxite-filled graben checked by drillings. *Fig. 68/a* shows the resistivity map ( $\rho_A$ ) constructed from channel 15 (2.2 ms).

To reduce exploration costs and to speed up the survey, CIL soundings can be replaced by Turam mapping (in the case of mapping, only the receiver is moving, the transmitter should not be relocated for each sounding). For the Turam mapping a resistivity calculation algorithm had to be elaborated which provides complete transient sounding curves in each mapping point for late times. *Fig. 68/b* shows the results of a mapping made within a  $400 \times 400$  m transmitter loop (channel 12, 1.1 ms). Similarly to the former one, this map provides the direction of the graben. The detectability of the small-size bauxite deposit under the inhomogeneous conductive overburden can be explained by the fact that the total longitudinal conductance variation affects transient measurements more than dc or frequency domain measurements (KAUFMAN 1978).

The examples shown prove the possibility of using transient measurements for bauxite exploration but several factors should be clarified. Promising results were achieved in the exploration of other raw materials and in structural investigation. Further works are planned for the development of interpretation methods.

## References

- ANDERSON L. 1981: Transient soundings for central-induction loop forward solutions for layered models. USGS Open-File Report, pp. 81–1309.
- KAUFMAN A. A. 1978: Resolving capabilities of the inductive methods of electroprospecting. *Geophysics*, **43**, 7, pp. 1392–1398.
- NABIGHIAN M. N. 1979: Quasi-static transient response of a conducting half space. *Geophysics*, **44**, 10, pp. 1700–1705.
- PRÁCSER E. 1986: Computing of transient response of layered halfspace, problems in apparent resistivity inversion. *Geophysical Transactions*, **32**, 3, pp. 221–234.
- PRÁCSER E., SZIGETI G., SZABADVÁRY L. 1983: Computation of multifrequency electromagnetic sounding curves ELGI 1982. Annual Report pp. 213–217.
- RAICHE A. P., GALLAGHER R. G. 1985: Apparent resistivity and diffusion velocity. *Geophysics*, **50**, 10, pp. 1628–1633.

## 2.2.2 New method for the exploration of solid mineral deposits of complex tectonics\*

While structural conditions in recently explored coal deposits are of ever increasing complexity, the demand for more detailed and accurate information, regarding tectonics, is growing. The detection of small amplitude structural elements, normal and reverse faults, pinch-outs is a rather difficult task not only for surface geophysical methods but even for the latest well-logging methods.

In recent years new methods have been developed for the exploration of larger spaces than the well-logging methods do. These methods provide higher resolution than the surface measurements. Although well-logging devices are required for the measurements, these are called cross-hole measurements, geotomography or down-hole measurements irrespective of being an electric or seismic method. The predecessor of these procedures is the *mise-à-la-masse* method.

In what follows, a variant of the electrical tomography, developed in the Soviet Union will be discussed. This method is called *geoelectric layer tracing*.

### *Theoretical basis for the geolectric layer tracing (GLT) method*

Let us suppose that the resistivity of the coal seams is higher by at least one order of magnitude, than that of the host rock and it hardly changes within the exploration area.

To carry out the measurements, two boreholes intersecting the coal seam and penetrating into the underlying layer, are required. The current electrode  $A^+$  is a point-like dc source, placed in one of the holes, while the other, the  $B^-$ , is at "infinite" distance from the borehole on the surface. At first  $A^+$  is in one of the boreholes and the  $\Delta V$  potential difference is measured in the other borehole with a stationary electrode pair. This measurement is repeated in various positions of the electrode  $A^+$ , above and below the coal seam as well. The most important is that a sufficient number of measurements should be carried out with the current electrode within the coal seam. After completing the measurements, the current and potential electrodes should be interchanged and a new set of measurements should be carried out. The simultaneous interpretation of the two measurement sets allows a more reliable evaluation of bedding characteristics of the coal seam between the two boreholes.

If both the current electrode and the reference point of the potential electrodes are in the plane of a continuous coal seam—this plane can also be tilted—the potential electrodes are on an equipotential surface, the potential

---

\* Király E., Szigeti G.

gradient is near to zero. This is true even if one of the boreholes has not intersected the coal seam or intersected it at a different depth because of a fault (in the case of a fault, that part of the seam is determined as the plane of the coal seam which is intersected by the borehole containing the potential electrodes). If the difference in the intersection depths is due to the dip of the coal seam, the zero places of the potential gradient can be used to determine the real dip of the layer.

Another feature of the potential field, yielding information on coal seams is whether potential gradient anomalies of similar shape change sign, when the current electrode passes through the coal seam. With the above two features, studied together, the continuity of the seam between two boreholes can be determined and the place and nature of the eventual discontinuity can also be established.

In practice, instead of the potential gradient, the potential difference closely approximating it is measured and for the above model the before mentioned features are valid with certain neglects only. The anomaly in the potential difference profile depends on the ratio of the real resistivity of the host rock and the coal seam. From among the geometrical characteristics, the ratio of the distance between the boreholes and the required exploration depth is of prime importance.

Beside the measured potential difference profiles, the so-called dipole potential profiles can also be used for interpretation. This can be constructed from the potential difference profiles by plotting the data measured with those potential electrodes having their reference points within the coal seam as a function of the depth of the corresponding current electrode. Based on the reciprocity principle, a profile is then obtained which could have been measured with a dipole source within the coal seam and a point-like potential electrode.

The qualitative interpretation, which is used for the determination of the spatial position of the coal seam, is carried out by comparison with the theoretical profiles calculated for the most important basic models.

### *Quantitative interpretation of GLT data*

Besides the qualitative interpretation it would be very important to determine resistivities of the coal seam and the host rock, and in the case of non-continuous seams the exact location of the discontinuity. This can be accomplished by calculating theoretical curves using the geometric configuration and dimensions of the given measurement and, by changing the resistivity values to get the best fit. Best results are provided by dipole potential profiles. The main reason for this is, that for the given model the measurement accuracy of the dipole potentials is the highest (in a layer of higher resistivity the potential differences are larger and thus they can be measured more reliably).

The theoretical potential difference and dipole potential curves are calculated for horizontally homogeneous models consisting of arbitrary number of layers. The theoretical solution allows the deviation of the vertical resistance from the horizontal one within the layers.

The algorithm used in the program calculates the kernel function of the solution obtained in Hankel transformed form using a stabilization procedure protecting against exponential overflow. The transforms are determined exclusively on the basis of the Weber–Lipschitz formula, with exponential approximation of the kernel function.

For the interactive interpretation, initial data are taken from the resistivity logs of the boreholes as the geoelectric layer tracing profile is significantly influenced by the immediate geoelectric vicinity, the resistivity distribution around the borehole. If by changing the parameters interactively a theoretical curve similar to the measured one can be obtained, it provides a quantitative evidence for the existence of an undisturbed, continuous seam between the boreholes. If it is impossible to reach a good agreement, this refers to the fact that the actual geological model significantly deviates from the horizontally layered one (i.e. from the one-dimensional model).

#### *Application of the GLT method*

Geoelectric layer tracing measurements have been carried out in the Dubicsány, Oroszlány and Mány coal exploration areas. The best results were obtained in the Dubicsány area, where the main characteristics of the geological structure could be determined from about 30 borehole pairs.

The profiles measured in the borehole pairs of the south western part of the Dubicsány area are shown in *Fig. 69*. It is striking, that anomalies suitable for interpretation can be found only at the upper seam of the deposit; at the lower seam the effect can hardly be detected, although in the averaged resistivity logs, the resistivities of the two seams are rather similar and differ only slightly from the resistivity of the host rock. The contradiction is only apparent. In reality the upper seam comprises brown coal of good quality and high resistivity, while the lower one is a clayey coal of lower resistivity, but this difference is not reflected by the average resistivity logs.

Based on the dimensions of the measuring configuration, the existing resistivity and thickness parameters, the limit of reliable layer tracing distance is 170 m, slightly less, than the actual distance. The zero crossing of potential difference curve No. 4 of borehole Pu-44 is at the depth of 77 m. From this value  $\lambda=1.4$  anisotropy can be calculated. The profiles show all the characteristics necessary for the interpretation. From the shape of the dipole potential profiles and from the places of zero crossings directly below the seam it can be concluded that the coal seam is continuous between the two boreholes.

Based on our experiences those areas can be selected for the coal mining industry with fair certainty where the coal seams are undisturbed, continuous, their dip is not very steep and the existence of a fault with a throw larger than the seam thickness can be excluded.

### 2.2.3 Hydrocarbon exploration by geoelectric methods\*

The low amplitude domes, where hydrocarbons accumulated in porous formations cannot be detected by geoelectric, or even by seismic methods of the highest resolution. Either the primary migration leading to the development of the deposits, or the secondary migration after the development of the deposits might have caused changes in the physical parameters of the overlying layers, which allow the direct detection of the presence of hydrocarbons by geoelectric methods, and the delineation of the deposits.

In what follows results of controlled source frequency soundings, magnetotelluric, self-potential and induced polarization measurements carried out over gas lenses of a few km diameter will be shown. These lenses can be found in Pannonian formations at the depth of 700 to 1200 m in the vicinity of Battonya. The measurements were carried out in the area described in Annual Report for 1983, and about 20 km from there around Kaszaper where the geological-geophysical model is similar. Measuring configurations are shown in *Figs. 70 and 71*.

Induced polarization measurements were carried out in the time domain. From the decay curves induced by current impulses of 15–20 s duration, at first the dynamic parameters are determined, i.e. the decay curves are approximated by the sum of exponential terms according to the following equation

$$U(t) = \sum w_i \cdot e^{-t/\tau_i} + w_0$$

where:

$w_i$  — amplitude of the  $i$ -th exponential approximating the decay curve;

$\tau_i$  — time constant of the  $i$ -th exponential term;  $w_0$  — constant.

*Fig. 72* shows the decay curve recorded at station 35 of profile KASZ-1 with electrode separation AB=1600 m (circles). The decay curve is the result of two different physical processes. The time constant of the electromagnetic induction process is shorter than that of the induced polarization, its amplitude is negative and under the given conditions it has a higher absolute value. Thus for about 0.3 s the effect of the EM coupling dominates and after this period that of the IP. For the above reason our decay curves are generally approximated by the sum of 2–4 exponential terms, 1–2 of them being EM (with negative amplitude), and the others IP (with positive amplitude) terms.

\* Csörgei J., Láda F.

Dynamic parameters are marked with an asterisk in the figure, and these values were determined by the Marquardt algorithm using HP 9845B computer. The curve calculated using the best fitting parameters is plotted with solid line in the figure. The measured (+) and calculated (solid line) values of the differential polarizability (dP) are also shown.

*Fig. 73/a* shows changes of the induced polarization parameters along profile BAT-1 obtained from decay curves measured with electrode separation  $AB=2400$  m. *Fig. 73/b* shows the apparent polarizability-time section, which is determined by subtracting the EM terms and the constant ( $w_0$ ) from the measured decay curve, then the remainder—the apparent polarizability values—are plotted along the profile as a function of time. It is clear, that the exponential amplitude ( $w$ ), the time constant ( $\tau$ ) and the apparent polarizability profiles show relative maximum–minimum pairs in the vicinity of the gas–water contact (stations 15–16, 18–19 and 25–26).

Five-component ( $E_{X1}$ ,  $E_{X2}$ ,  $H_{Y1}$ ,  $H_{Y2}$ ,  $H_Z$ ) controlled source frequency soundings were carried out using a special configuration for the investigation of local inhomogeneities of the sequence at 300–1200 m depth. The measurements were carried out with the ERSz-67 generator station (maximum 30 A current) and DEF-1 digital equipment in the 1–30 Hz frequency range (104 discrete frequencies at each sounding), using an array close to the dipole equatorial.  $AB=2000$  m and  $AB=2500$  m grounded electric dipoles were used as sources, the electric field parallel to the transmitter dipole ( $E_X$ ) was measured with receiver dipoles of  $MN=100$  m, the vertical magnetic field and that perpendicular to the transmitter dipole ( $H_Z$  and  $H_Y$ ) were measured with induction coils, up to 1000–1250 m separation from the equator of the transmitter dipole, in both directions. The separation between the transmitter and receiver lines (R) was 6–8 km (*Fig. 71*), which is large enough to carry out the soundings in the near-field zone if the applied frequency range and measured apparent resistivities are considered. Thus the reference point of the controlled source measurements is at the site of the receiver. The deviations from the dipole equatorial array were corrected for in the processing with the geometric coefficients.

Processing of the measurements was carried out with R-35 and HP 9845B computers. From the individual sounding curves apparent resistivity–depth sections were constructed, then using the procedure discussed in the Annual Report for 1983 these sections were separated into a regional and a residual part. *Figs. 73/c, d* and *e* show section BAT-1 in the 350–900 m depth range (approximated by  $N=2$  and  $K=10$  grade polynomials, against *Fig. 52* of Annual Report for 1983, where  $N=5$  and  $K=10$  were used). In the apparent resistivity section a monotonous decrease can be observed downwards, while in horizontal direction only small resistivity changes occur. In the residual anomaly section anomalies occur at 700–800 m depth around stations 0, 15, 19 and 26, coinciding with the IP anomalies.

The parameter changes occurring in the vicinity of non-structural hydrocarbon deposits — mainly geoelectric inhomogeneities, „chimneylike” resistivity and induced polarization changes above or at the boundaries of gas lenses — and some Soviet case histories led us to the decision, that magnetotelluric soundings should be performed in such environment. Measurements were carried out with digital magnetotelluric instrument DEF-1, in the 0.5–20 Hz frequency range (Fig. 71), using  $MN=100$  m electrode separation and 200 m station separation (shorter electrode separations are prohibited because of the electric parameters of the instrument). Similar to the controlled source frequency soundings it was not expected, that magnetotelluric measurements could be used for the determination of geoelectric layers from individual sounding curves, but the changes of the natural electromagnetic field along the profile was to be followed. Computation of magnetotelluric impedance values was carried out by a R-35 computer using the standard processing program developed in ELGI earlier, with time domain convolution filtering. The impedance and magnetic polar diagrams were plotted with a HP 9845B computer.

*Fig. 74* shows results of measurements carried out earlier along profile BAT-3. In spite of the penetration depths belonging to 10–20 Hz frequencies (a few hundred meters) do not reach the depths of gas-bearing layers ( $\sim 750$  m), the polar diagrams indicate horizontal inhomogeneities, two- and three dimensional geoelectric structures. Above horizontally layered medium the impedance polar diagrams are of circular shape, while the values of the magnetic tensor describing the relation between the vertical and horizontal components of the magnetic field are a few hundredths only. In our case, however, near to stations 11 and 21—in the vicinity of the gas–water contact—the impedance polar diagrams are significantly distorted. It can be seen from the magnetic polar diagrams that the values of the tensor approximate and even exceed 1, i.e. the vertical magnetic changes can be compared with the horizontal ones. This also confirms our opinion, that geoelectric parameter changes might occur not only in the close vicinity of hydrocarbon deposits, but at much shallower depths too, as a result of geochemical processes associated with the migration of gas.

To create an acceptable geological–geophysical model, the geoelectric methodological experiments should be completed with metallometric analysis of the core samples (or drilling mud) and IP logging in exploration or production wells. Comparative investigations should be carried out in barren areas too using both surface geoelectric measurements and downhole investigations.



## 2:2:4 Methodology of engineering geophysical sounding

### *The potential applications of engineering geophysical sounding in planning of open pit lignite mining\**

The Mátraalja Coal Mines produces lignite by open pit mining. During the fall of 1985 we had the opportunity to carry out experiments in the area designed for stripping, using the present routine engineering geophysical sounding technique to determine the lithology of the overburden, the depth and quality of the lignite seam, further the filtration coefficients of the various formations in the intersected sequence.

The penetration depth was between 15 and 21 m, and the separation between the soundings—11 along a profile—was 20 m (*Fig. 75*). The value of the filtration coefficient was determined in 6 soundings, in 9 formations of different quality. The overburden was completely intersected at each sounding, but information was obtained only from the upper 1.5–7.0 m of the lignite seam. The values of the filtration coefficient and the groundwater conditions along the profile were also determined.

Although the upper sequence of 10.5–15.8 m thickness comprises mainly clay, sounding 1 shows alternating semi-impermeable and semipermeable interbeddings of fluvial origin. On the surface a temporary stream can be found even now. Our measurements indicate layers of mixed grain size in soundings 4, and 6 to 9. From sounding 1 to 5 the lignite is overlain by a clay of very high plasticity, further along the profile this clay can be found within the overburden. Except sounding 3 this clay layer is 1.0–2.1 m thick. Its natural radioactivity—measured by the given nuclear instrumentation—is about two times higher than that of formations generally identified as clays. Practically it has no mechanical—compression and shear—strength, during the penetration of the probe it behaves like a fluid of high viscosity. The extreme values of the bulk density are 2.02 and 2.26 t/m<sup>3</sup>. During stripping of the overburden the stability of the slope is significantly endangered by the plastic clay. One of our most important results is the reliable detection of this layer, which is rather dubious by drilling.

Our investigations have proved that the surface of the lignite formation can be determined accurately by engineering geophysical sounding, because it means a 0.7–0.8 t/m<sup>3</sup> decrease in the bulk density, and 75–80% decrease in the natural gamma activity (in the case of a clay–lignite contact). The bulk density of lignite is 1.32–1.45 t/m<sup>3</sup>. At soundings 1 to 6, there is a transitional sequence of 1.0–3.3 m thickness, immediately overlying the lignite. This contains 20–30 cm thick interbeddings with peak pressure and natural gamma activity decreasing or increasing simultaneously. Further studies are required for the determination of their lithology.

---

\* Dobrovolni K.

By revealing the hydrologic conditions valuable information is provided for planning the drainage of the mining pit. The static groundwater table in the impermeable overburden has developed under pressure. The filtration coefficient of the lignite is by 7-9 order of magnitude higher than that of impermeable clays. Therefore drainage of the lignite should be commenced already during stripping of the clay, because at the critical thickness of the overburden as a result of hydraulic soil failure, or as a consequence of stripping off the top of a lignite dome, confined groundwater might flood the pit.

In spite of the above described results, further development of the method is required for investigating the lignite itself.

### *Computer-aided interpretation of engineering geophysical soundings\**

The engineering geophysical sounding method has gained more and more important role in the exploration of loose near-surface sediments. The increase in the amount of measured data required the introduction of computer-aided determination of layer boundaries and automatic identification of layers. The program described below, and shown in the flow chart of *Fig. 76*, can be run on a Commodore 64 computer. It determines the lithological column and produces a graphic plot from four sets of field data (total pressure, peak pressure, gamma-ray and gamma-gamma radiation).

Processing and interpretation of measured data are carried out in several steps as shown in the flow chart:

1. During data preparation most of the errors are removed from the recorded data with one-dimensional filters. The errors might be individual ones (occurring in the measuring process), or might be statistical ones (fluctuations resulting from the statistical nature of the gamma radiation and the microstructure of the layers).
2. Based on the corrected data, determination of the layer boundaries is performed in two steps. At first, places of largest changes are sought for in each channel, then—based on a combined evaluation of the information in all four channels—the program selects the zones which can be interpreted as layer boundaries. The various channels are weighted differently in the selection. Weighting is determined by the importance of the channel in layer boundary determination, on the one hand, and by the necessary and sufficient changes in the measured values of the channels for the unambiguous recognition of lithological changes, on the other.
3. Calculation of the parameters, characteristic for the individual layers, is carried out by simple averaging; transition zones are not taken into account.

---

\* Fejes I.

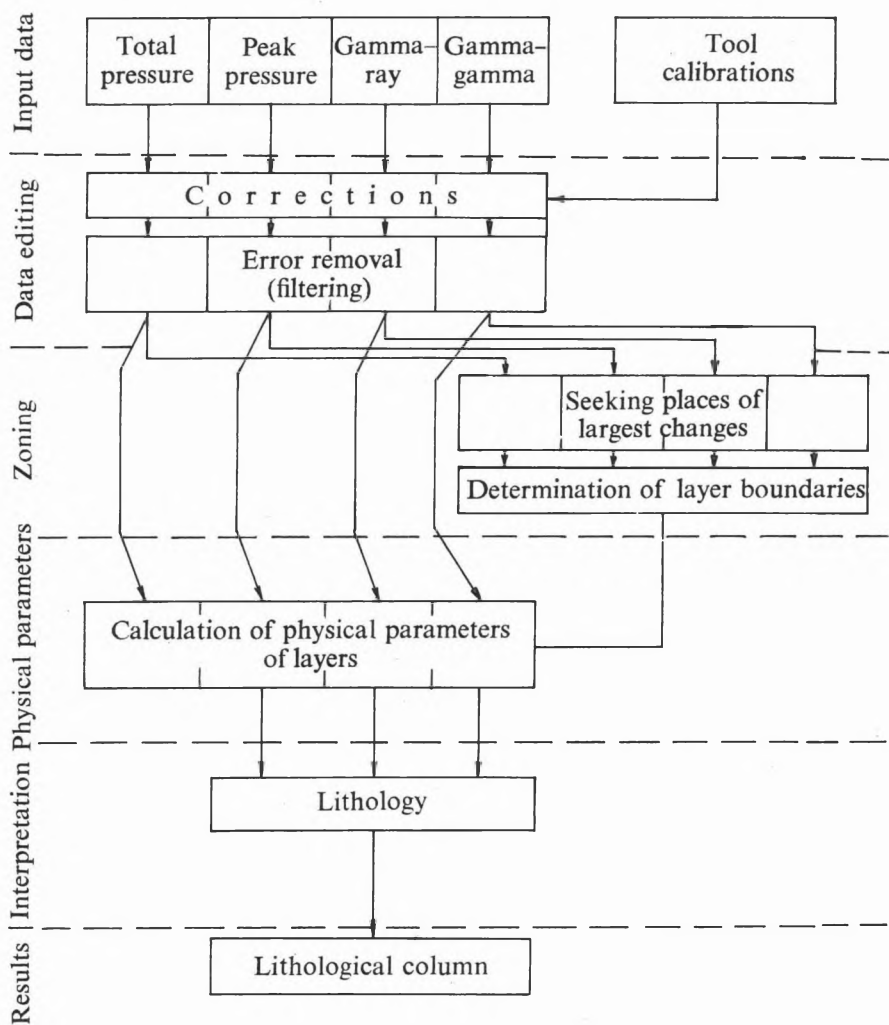


Fig. 76. Flow chart of computer processing of engineering geophysical sounding data

4. For the time being the program is able to interpret, i.e. to identify alluvial formations only. We have gained most of our experience in the investigation of these types of lithology, therefore the computer was taught for the recognition of these formations. If the three main parameters (the peak pressure being proportional to the breaking strength, the natural gamma activity proportional to the clay–mud content, and the gamma–gamma value proportional to the bulk density) are plotted along the axes of a spatial coordinate system, the parameters of a given layer determine a spatial point. According to our measurements the basic lithologies are characterized by more or less wide ranges of parameters, i.e. space compartments in our coordinate system (*Fig. 77*). These compartments of the space are well separated from each other. Based on the distance between the point determined from an individual measurement, representing an actual layer and the centre of gravity of the space compartments determined by the measurements representing various formations it can be decided, which of the formations lies the nearest to the measured data trio.

Based on our experiences, the lithological column is determined fast by the computer. Although minor improvements might be necessary, the lithological column determined from objective criteria provides a sound starting point for the geophysicist, who performs the final interpretation.

### **2.2.5 Field data loggers and preprocessing units for geoelectric instruments\***

In 1985, ELGI developed a field data logger for her D–10R resistivity meter, and—using a pocket computer—a general purpose data logger and preprocessing unit for electromagnetic instruments (e.g. Maxi-Probe, EM–31).

The D–10R instrument directly measures a geophysical parameter, the apparent resistivity. The different resistivity techniques require different processing and therefore data acquisition and processing should be separated. For example, in the case of geoelectric layer tracing (see Section 2.2.2) in a single pair of boreholes several hundred data should be recorded in one day and between two consecutive readings a difference of even two orders of magnitude might occur. The measurements should be carried out fast (from the viewpoint of drilling, the measurement is dead time) and without error and the same applies for the field records.

The block diagram of the data logger is shown in *Fig. 78*. Its most important part is the 2 kbyte memory (M) consisting of CMOS RAMs. In the memory the average of repeated readings should be stored. Therefore the serial data, the measured  $\rho$  values, are transferred to a buffer memory (B), where 2, 4 or 8 readings are stacked. After giving the START command the average is calcu-

---

\* Simon P., Verő L., Vincze L.

lated (D), then the averages are transferred into the memory in the form of 3 decimal characters with a label or a serial number automatically increasing from 0 to 999. To determine the order of magnitude of the  $\rho$  value, the gain (A), set on the instrument, should also be stored. In the memory this is placed before the respective average value in the form of a code.

For data processing other information (e.g. the electrode configuration, repeated measurement, etc.) is stored in the form of a decimal code (from 0 to 9) as a sublabel (L), set by a thumb wheel.

Wrong data transferred into the buffer memory can be cancelled, but data in the memory cannot be overwritten, even by mistake.

The whole data logger consists of a single printed circuit board and it is mounted into the lid of the instrument. It is fed by 4 miniature rechargeable batteries. After turning off the instrument the memory is in stand-by state, the consumption becomes very low and data can be stored in the memory even longer than 6 months.

Our plan is to equip the D-10R instruments with two data loggers. While one of them collects the data in the field, the other is in the field office and through an interface (IF) the stored data are transferred into a PTA-4000 pocket computer (Sharp PC-1600 Pocket Computer). The capacity of this pocket computer is satisfactory for processing of dc geoelectric measurements.

The requirements set by the Maxi-Probe electromagnetic frequency sounding instrument having been used for years are somewhat different. The cost of this instrument is more than ten times higher and the data providing geological information should be calculated from the data measured by the instrument. This way the PTA-4000 pocket computer can be economically used both for data acquisition and storage and using its KA-160 printer-cassette recorder and IFSP serial-parallel interface a field system providing certain processing and displaying possibilities can also be built. This system is not so closely fitted to a given instrument like the data logger of the D-10R and can be easily connected to various geophysical instruments. The properties of the PTA-4000 explain the fact, that the same computer might be used for field data acquisition and storing with more expensive instruments and as a "big computer" with cheaper instruments. Its most important advantage for instrumental purposes is, however, that the complete bus system of the CPU is accessible through a 60-pole connector.

Connection of commercially available units of the general purpose field data acquisition and processing unit is shown in *Fig. 79*. Geoelectric instruments, of course, cannot be directly connected to the bus of the CPU. Considering the instruments and the processing tasks, interfacing of the multichannel analog port and several, 8-bit parallel digital input and output ports further the data memory to the bus of the CPU had to be solved and the main memory area had to be extended. The main memory of the computer has a capacity of

18 kbyte and further 10 kbyte storage built up of CMOS RAM elements was added, thus 28 kbyte maximum operating memory capacity has been reached. A 128 kbyte capacity data memory RAM can also be used.

Most of the geoelectric instruments have analog outputs, correspondingly data loggers should have analog inputs as well. The analog input uses an 8-channel analog multiplexer, but the number of channels can be increased. A 12-bit analog-to-digital converter is used, the integration period is 20 ms for the suppression of power line noise, the conversion time is 80 ms. The setting of the different switches of the instruments, further the control signals can be input through 8-bit digital ports. At present two such inputs are provided, but the number of these can be easily increased. The digital output is used for addressing the analog multiplexer, but it can be used for measurement control and display purposes too.

Figure 79 shows the data logger (DL) interfaced to a Maxi-Probe instrument. The instrument measures the real and imaginary parts of the horizontal and vertical magnetic components of man-made electromagnetic field relative to an internal clock at many frequencies and produces direct voltages proportional to these four field parameters. From these direct voltage levels analog circuits generate the quantities required by the processing, and these can be read from a pointer instrument. The data logger and preprocessing unit takes over the function of these analog circuits and the pointer instrument. It carries out the arithmetical operations more accurately than the analog circuits and at the same time it automatically stores other data required by the processing too (gain of the two input channels, measuring frequency).

In Maxi-Probe measurements on-site plotting of the sounding curves is frequently desirable. Fitting of the selected measuring parameters to the given geological model can be checked only using these curves. Such a curve plotted in the field is shown in *Fig. 80*. Using the keyboard of the computer any header can be compiled. It is more important, however, that using repeated readings the accuracy of the measurement can be increased by digital filtering. These operations and the processing itself, further the graphic displaying requires a rather long program and this necessitated the extension of the memory of the computer to the maximum capacity.

A more simple task was the interfacing of the data logger to the EM-31 conductivity meter. The signal proportional to the conductivity of the soil is indicated by a pointer instrument, but there is an output for an analog recorder too. The data logger is connected to this output, the real and imaginary parts of the measured signal are input into two analog channels, and the gain setting is transferred into the digital input.

Storing data on tapes, and connection of the PTA-4000 to desk-top computers (HP 9845)—as in the case of D-10Rs—allow further processing and more sophisticated representations.

## 2.3 WELL LOGGING INSTRUMENTAL AND METHODOLOGICAL RESEARCH

### 2.3.1 Photoelectric index logging\*

In the year covered by the report investigations were carried out with the purpose of laying the foundation for introducing the photoelectric index ( $P_e$ ) logging. The photoelectric index can be determined by analysing the spectrum of back-scattered gamma radiation of rocks [BERTOZZI et al. 1981]. Since the photoindex is a strictly monotonous function of the atomic number, it furnishes information on general chemical composition and through it on the quality of rocks.

When the chemical composition is known, the photoindex of the rock can be calculated. For a certain rock type, of course, the photoindex varies within a certain range because of the variation of chemical composition. Photoindex intervals of various rocks and several compounds are listed in *Table II*. Low photoindex values between zero and two are given by coal, as well as water or oil- and gas-bearing sandstone, intermediate values between two and ten may correspond to a multitude of rocks, thus they are not informative by themselves. Photoindex values over ten are indicative of metalliferous rocks. However, intermediate photoindex values may also provide useful information when combined with other data, as it is illustrated in Figs. 81 and 82.

In *Fig. 81* the photoindex of several simple systems of two components can be seen vs. porosity. The pore liquid was accounted for as water, but if the pore space is filled up with oil, the photoindex does not change significantly, since water and oil have nearly identical photoindices. If it is known from preliminary investigations that any of the illustrated three rock matrices comes into the plot, then the photoindex enables us to decide which one is involved in the given case.

In *Fig. 82* the photoindices of clays and bauxites are presented vs. combined iron oxide content. Besides the low atomic number components the percentage ratio of iron having a comparatively high atomic number plays a decisive role in forming the average atomic number. There is a fairly good correlation between iron content and photoindex. The determination of iron content may contribute to increasing the accuracy of testing of bauxites for quality.

---

\* Buránszki J.

Rock or material	Photoindex minimum	Photoindex maximum
Water	0.358	
Oil	0.125	
Coal	0.16	0.2
Granite	2.4	2.9
Sienite	3.4	5.1
Gabbro	3.5	6.5
Dike rocks	2.3	5.3
Basalt, diabase, melaphyre	4.6	6.4
Clay	1.5	5.0
Bauxite	5.0	6.3
Sandstone	1.7	2.7
Shale	2.7	5.8
Limestone	4.5	5.2
Dolomite	3.1	3.6
Gneiss	2.1	4.1
Amphibolite	4.6	6.3
Serpentinite	2.7	3.5
Iron ores	10.0	16.0*
Manganese ores	8.0	16.0

\* The  $P_0$  of barium containing iron ores may be as high as 30 to 60.

Table II. Photoindex intervals of rocks

According to our examples the photoindex as a new geophysical parameter of well logging permits to check density logs in coal exploration as to the correctness of determination of layer boundaries, while in hydrocarbon or water exploration it permits to achieve a more accurate estimation of density and porosity through the identification of reservoir rocks and to determine the iron content of bauxites.

#### References

BERTOZZI et al. 1981: The physical foundation of formation lithology with gamma rays. *Geophysics* **46**, 10, pp. 1439-1455.



### 2.3.2 Computerized interpretation of coal exploration wells

#### *Application of the ASOIGIS system\**

The computerized well logging analysis system (ASOIGIS) established as the result of one and a half decade's cooperation within the framework of the Council for Mutual Economic Aid was designed for the purpose of hydrocarbon exploration. In 1985 this system was introduced into the interpretation of coal exploration wells. The procedure of processing is shown on logs measured in a borehole of a lignite field in the northern part of Hungary. The processing includes the following main steps:

#### Relative depth matching of logs

The program which performs relative depth matching approximates depth differences of logs point by point by a polynomial. When the log to be matched ( $y_1(x)$ ) is expanded in a Taylor series according to depth, the depth differences correspond exactly to substitution values of the polynomial  $\Delta(x)$ . By minimizing the quadratic differences of the log expanded in series and the linear combination of the rest of logs ( $y_2, y_3, \dots, y_n$ ), the coefficients of the polynomial can be determined.

$$y_1(x) + \Delta(x)y_1'(x) = a_2y_2(x) + a_3y_3(x) + \dots + a_ny_n(x)$$

$$\Delta x = b_0 + b_1x + \dots + b_px^p$$

$$\int [y_1(x) + \Delta(x)y_1'(x) - (a_2y_2(x) + a_3y_3(x) + \dots + a_ny_n(x))]^2 dx = \min.$$

When they are substituted back into the Taylor series, the values of the corrected log can also be received. This procedure is repeated several times for each log, making the calculated values converge toward the respective values of the already matched logs. The program permits to match all logs simultaneously or to take a few as basic logs and to match the rest to them. Logs of the presented borehole matched according to depth are shown in *Figs. 83 and 84*.

#### The use of special crossplots

Calibration of measurements for accurate physical values and determination of parameters characteristic of rock components are made by using special crossplots. When the logs are being taken for probability variables, through utilizing their measured values and standard deviations which in turn are dependent on their difference ratios, one can calculate the probability of

---

\* Szendrő D.

their belonging to individual rectangular domains of the coordinate system. Thus, for two logs, a two-dimensional, integral probability distribution is obtained. With a third log being taken into consideration, one can form the weighted averages for the individual rectangular domains, in which the weights are directly proportional to probabilities determined from the previous two logs in the discussed manner and inversely proportional to the quadratic standard deviations of the values of the third log. An example of the former, so-called probability plot is presented in *Fig. 85*, and of the latter, so-called ZW plot in *Fig. 86*, with the encountered rock components being indicated.

### Statistical lithological interpretation

The statistical lithological interpretation is carried out for each sampling point. It requires the matrix of lithology characteristic for the area, which contains the lower and upper limits of geophysical parameters pertaining to the given logs and rock types, as well as the probabilities of the occurrence of individual rock types. Using a conditional probability, the program calculates—from the measured values and their standard deviations—the probability of the measured value, using the ranges defined in the matrix of lithology. Forming the resultant probabilities for each type of rock from several logs, the program indicates the rock type having maximum probability. This result of the statistical lithological interpretation can be seen in the far right column of *Fig. 84*.

### Determination of rock components

Rock composition can be determined from a system of equations to be written for each depth point for the measured neutron porosity, density, resistivity and gamma-ray log. The program solves the non-linear system of equations—whose parameters are defined by cross-plots—using an iteration for the unknown volume percentage. The calculated rock composition in volume percentage is given in the left column of *Fig. 87*.

### Calculation of quality parameters

When it is assumed that the ash content of coals is mainly due to solid components of the embedding rocks, and the moisture content can be defined as the sum of calculated effective porosity and of the content of bound water in the barren rock, the determination of coal, ash content and moisture in weight percentage is illustrated in the central column of *Fig. 87*. If the combustion heat of the given coal type is known, the caloric value can be obtained by subtracting the amount of heat required to warm up the water—to its

weight percentage in proportion—from the combustion heat of the coal multiplied by its weight percentage. The caloric value is plotted in the right column of Fig. 87.

The program system works in routine operation and, as experiences show, the obtained results—in agreement with traditional interpretation—furnish useful information for delineating coal fields and for decomposing the lithological complex. In addition, by deducing quality parameters of coals solely from geophysical measurements, the system helps to reduce the expensive coring to a minimum.

### *Interactive processing with minicomputers\**

An improved version of the program system discussed in the Annual Report for 1984 (p. 197) permits to determine the conditions of overlying and underlying rocks of coal beds. Laboratory grain distribution curves offer a means to calculate the filtration coefficients of overlying and underlying formations.

Effective grain diameters ( $D_{10}$ ) determined from laboratory grain distribution curves can be brought into correlation with nuclear logs. Closest correlation is observed with the relative gamma log (R-GAMMA) calculated from the gamma-ray log. By the aid of this correlational relationship, described by a third-degree polynomial (Fig. 88), a continuous  $D_{10}$  curve can be created. With the  $D_{10}$  curve known, the  $k$  filtration coefficient is calculated from the function with two variables  $k=f(\Phi, D_{10})$  established for the given exploration area, where  $\Phi$  is the value of effective porosity in per cents. Filtration conditions of the penetrated section are well reflected on the calculated  $k$  curve. Fig. 89 shows the relationship between filtration coefficient and neutron porosity, with  $D_{10}$  as parameter. Results obtained through processing data of an exploratory well at Dubicsány are presented in Fig. 90.

A branch of this program system dealing with filtration conditions can be used to interpret logs measured in wells of water exploration which penetrate formations composed of clay and sand; investigations in this field started already.

### **2.3.3 Well logging instrument development\*\***

For the determination of filtration and reservoir parameters of productive hydrocarbon- and water-bearing layers hydrodynamical methods are used. Among the parameters down-hole pressure- and temperature measurements are of utmost interest. To render these measurements possible, the KPT-2-

---

\* Karas Gy., Bihari A., Mészáros F.

\*\* Korodi G., Szentpály M., Vadász G., Lakatos S. (VIKUV)

120-43Y sonde was designed by which pressure and temperature can simultaneously be measured. The operating principle can be seen on *Fig. 91*. The pressure gauge (1) consists of strain gauges glued on a planar diaphragm built as a Wheatstone bridge. The bridge is zero positioned and temperature compensated. The output voltage of the bridge (of mV order of magnitude) that is proportional to the pressure is amplified by a high stability amplifier (3). The output voltage is converted by an ultralinear voltage/frequency converter (4) thus the output frequency is proportional to the pressure. The temperature gauge (2) is a special integrated circuit with a time constant of 1.5 s in liquids. Its characteristic is fixed to the absolute temperature and is linear within  $\pm 0.5\text{ }^{\circ}\text{C}$  so the sonde has to be calibrated only once. The signal of the temperature gauge is processed also by a voltage/frequency converter (4). The signals of both the temperature and the pressure channels come to a logic circuit (5) which eliminates the pulse coincidence. The pressure and temperature signals reach the surface in the form of positive and negative pulses on a single conductor. In order to achieve maximum stability the electronics of both the temperature and the pressure channel are operated from a high stability power supply unit.

The mechanical construction of the sonde can be seen on *Fig. 92*. It is of 1470 mm in length, 43 mm in diameter and is made of corrosion-resistant steel. The pressure- and temperature sensors form one unit in a protective cage providing rapid temperature exchange. Processing of the pulses and the power supply of the sonde are provided by the surface unit of type KFU-4-12P. It is based on a microprocessor of type Z-80 with a 16 kbyte operative memory providing considerable flexibility. According to the burnt-in program it computes the temperature and pressure values from the input pulse counts, and displays them on 4 analog outputs and on a 16-character alphanumeric display. Moreover it compensates for the temperature drift of the pressure channel as well as performs the calibration of the temperature and pressure channels. With a connected matrix printer the curve can be displayed in time logarithmic scale as well. On *Fig. 93* a pressure recovery curve and its repetition can be seen (Göd,  $T_{amb} = 56\text{ }^{\circ}\text{C}$ ,  $P_{abs} = 50\text{ bar}$ ).

Features for temperature measurements:

measuring range	120 $^{\circ}\text{C}$
absolute accuracy	$\pm 1\text{ }^{\circ}\text{C}$
resolution	0.05 $^{\circ}\text{C}$
time constant	2 s

For pressure measurements:

measuring range	300 bar
absolute accuracy	$\pm 0.5\text{ bar}$
resolution	0.03 bar